Received: 10 February 2017 | Revised and accepted: 3 October 2017 | Uncorrected manuscript published: 5 October 2017 | Published on: 7 November 2017

DOI: 10.1111/tra.12532

WILEY Traffic

ORIGINAL ARTICLE

Membrane lipid order of sub-synaptic T cell vesicles correlates with their dynamics and function

George W. Ashdown[1] | David J. Williamson[1] | Gary H.M. Soh[2] | Nathan Day[1] | Garth L. Burn[3] | Dylan M. Owen[1]

[1]Department of Physics and Randall Division of Cell and Molecular Biophysics, King's College London, London, UK

[2]Friedrich Miescher Laboratory, University of Tübingen, Tübingen, Germany

[3]Max-Planck Institute for Infection Biology, Berlin, Germany

Correspondence
Dylan M. Owen, Department of Physics and Randall Division of Cell and Molecular Biophysics, King's College London, London, UK.
Email: dylan.owen@kcl.ac.uk

Funding information
H2020 European Research Council, Grant/Award number: 337187; Marie-Curie Career Integration, Grant/Award number: 334303

During an immune response, T cells survey antigen presenting cells for antigenic peptides via the formation of an interface known as an immunological synapse. Among the complex and dynamic biophysical phenomena occurring at this interface is the trafficking of sub-synaptic vesicles carrying a variety of proximal signalling molecules. Here, we show that rather than being a homogeneous population, these vesicles display a diversity of membrane lipid order profiles, as measured using the environmentally sensitive dye di-4-ANEPPDHQ and multi-spectral TIRF microscopy. Using live-cell imaging, vesicle tracking and a variety of small molecule drugs to manipulate components of the actin and tubulin cytoskeleton, we show that the membrane lipid order of these vesicles correlate with their dynamics. Furthermore, we show that the key proximal signalling molecule Linker for Activation of T cells (LAT) is enriched in specific vesicle populations as defined by their higher membrane order. These results imply that vesicle lipid order may represent a novel regulatory mechanism for the sorting and trafficking of signalling molecules at the immunological synapse, and, potentially, other cellular structures.

KEYWORDS

Vesicle, Membrane order, T cell, Synapse, Live Cell, Dynamics, Cytoskeleton

1 | INTRODUCTION

The T cell immunological synapse (IS) is a well-studied cell-cell junction that, after stimulation via T cell receptor (TCR) engagement, displays a high degree of cellular and molecular level reorganisation. After initial signalling through molecules residing within the plasma membrane (PM), a prolonged stage of secondary signalling is required for full synapse formation and maintenance.[1,2] This secondary signalling event relies on the recycling and redelivery of molecules to the interface and is important for supporting and balancing subsequent downstream signalling and T cell activation.[3,4] Vesicles form an important component of this molecular delivery and recycling machinery, with their dynamics and transportation mediated by active cytoskeletal components.[5] These mechanisms are speculated to include myosin transport along actin tracks,[6] actin polymerisation[7] and/or transport along microtubules.[5] F-actin modulates vesicle trafficking via myosin motors[8] and cargo fusion.[9] The cytoskeleton also creates hotspots of vesicle exocytosis in an actin and microtubule-dependent manner.[10]

Vesicle trafficking within T cells may rely on different cytoskeletal components as vesicles distribute to different synaptic regions such as the synapse centre or the periphery.[11] Additionally, these vesicles contain proteins responsible for organising their own trafficking, such as myelin and lymphocyte protein (MAL) which promotes vesicular relocation to the synapse interface.[11] Furthermore, molecules important for T cell activation such as Linker for Activation of T cells (LAT) have been associated with vesicular populations and sustained signalling from signalosome formation.[12,13] It has also been shown that TCR recycling and exocytosis may occur, which is speculated to control the level of TCR at the interface and therefore the strength of signalling.[14]

The PM is not a homogeneous environment and is thought to be comprised of co-existing and immiscible fluid lipid phases; the liquid-disordered phase and the liquid-ordered phase. The liquid-ordered phase is enriched in cholesterol, sphingolipids and saturated phospholipids, displays highly ordered lipid tails, higher lateral viscosity and a thicker bilayer.[15] Such ordered-phase domains have been shown to

© 2017 John Wiley & Sons A/S. Published by John Wiley & Sons Ltd

be important for lipid-regulated sorting during vesicle formation at the trans-Golgi network.[16] Proteins are partially partitioned between the two phases depending on the nature of their membrane-targeting sequence such as acyl post-translational modification or the length of their transmembrane domains.[17,18] Protein segregation or co-localisation may modulate protein signalling events within the IS with both LAT and MAL shown to be targeted to ordered-phase regions.[19–21]

Here, we hypothesize that like the PM, sub-synaptic vesicles possess differential membrane lipid order and that if so, these differences may be functionally important. We employ the environmentally sensitive membrane probe di-4-ANEPPDHQ which changes its fluorescence emission spectrum based on the order of the membrane in which it resides.[22,23] T cells can be imaged and analyzed using multispectral confocal and total internal reflection fluorescence (TIRF) microscopy allowing the order of individual vesicles to be quantified. By tracking the vesicles using live-cell microscopy, we show that different populations of vesicles do indeed exist at the T cell synapse and that their degree of membrane order correlates with their dynamic behaviour. This was shown to be related to their differential interactions with cytoskeletal components. Finally, we show that the membrane order of individual vesicles also correlates with those vesicles' protein cargo, including LAT.

2 | RESULTS

2.1 | Vesicles possess different membrane order which correlate with their dynamics

Primary human T cells were stained with di-4-ANEPPDHQ, washed and imaged using 2-channel TIRF microscopy while forming synapses against a stimulatory coverslip (see *Methods* section). Compared to control cells, which demonstrated no spreading and little to no fluorescence signal under TIRF illumination (Figure S1, Supporting information), cells stimulated on an antibody-coated coverslip exhibited clear vesicular structures. A representative movie of one of these time-lapse acquisitions is shown in Supplementary Movie 1. Figure 1A,B show raw images acquired from the blue-shifted (ordered) and red-shifted (disordered) channels followed by the pseudo-coloured generalized polarisation (GP) image (Figure 1C), which represents the degree of membrane lipid order. Individual vesicles were then identified and tracked, with tracks colour-coded by calculated GP values. GP values of individual vesicles were then correlated to their dynamics to establish the relationships between membrane order and vesicle behaviour (Figure 1D).

Pearson's correlation analysis of vesicle GP values vs vesicle track speed in these cells revealed a significant negative correlation (R^2 = −0.048, P < .0001, Figure 2A). Overall, these results indicate individual vesicle order may affect their dynamics, with more ordered vesicles moving slower. The finding that membrane lipid order correlates with vesicle dynamics provide the novel possibility that order may influence vesicle trafficking, potentially through differential interactions with the cytoskeleton.

As membrane dyes do not segregate specifically into vesicles alone, tracking experiments were repeated with Jurkat T cells transiently expressing an endoplasmic reticulum (ER) or Golgi marker to ensure these organelles were not being mistaken for vesicles. MAL-mCherry was also transiently expressed and tracked. Tracking results are shown in Figure S2, demonstrating ER, Golgi and MAL speeds are all significantly slower, possess shorter track lengths and exhibit straighter tracks (P < .0001 in all cases) compared with control vesicle statistics. Representative examples of time-lapse movies of the ER stain, Golgi stain and MAL are shown in Supplementary Movies 2-4.

If components of the cytoskeleton do indeed regulate these vesicle dynamics, disruption of these may change vesicle behaviour in an order-dependent fashion. This was investigated through the use of cytoskeletal perturbing drug treatments. Cells forming synapses against antibody-coated coverslips were treated with drugs to affect the actin and microtubule cytoskeletons. Cytochalasin-D and Jasplakinolide, respectively, disrupt and stabilize actin fibres while Nocodazole disrupts microtubule formation. Imaging of vesicles within primary human T cells was repeated after treatment with these drugs with results from Cytochalasin-D (Figure 2B), Jasplakinolide (Figure 2C) and Nocodazole (Figure 2D) displayed. The correlation between vesicle GP values and velocity was compared to control cells (which exhibits a −0.95 to −0.84 gradient value; 95% correlation confidence interval, CI) and was found to be significantly different for Cytochalasin-D (gradient between −0.58 and −0.41; 95% CI) and Nocodazole (gradient between −0.62 and −0.38; 95% CI)-treated

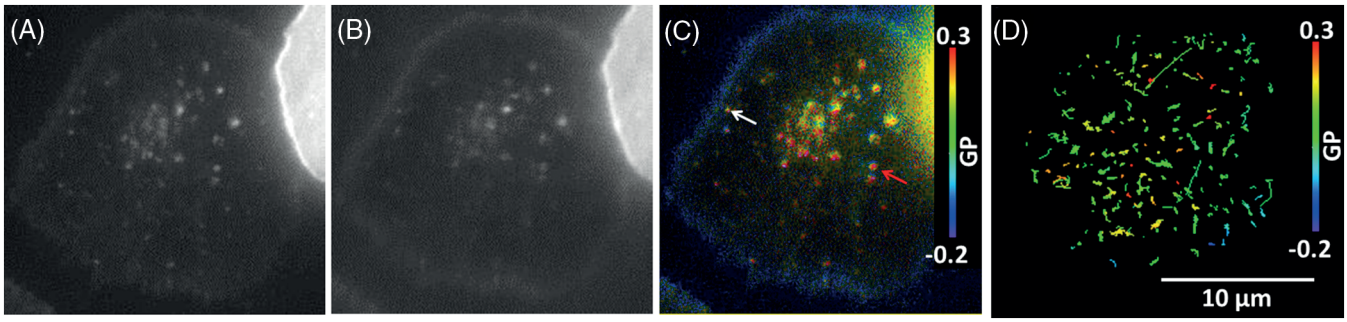

FIGURE 1 Imaging membrane lipid order in primary human T cell sub-synaptic vesicles. Representative T cell stained with the membrane dye di-4-ANEPPDHQ forming an immunological synapse when imaged in the green (ordered, A) and red (disordered, B) channels. (C) Psuedo-coloured image of GP values with white and red arrows indicating examples of more ordered and disordered vesicles, respectively. (D) Tracking of individual vesicles from a single, representative cell with tracks coloured by GP (order) value

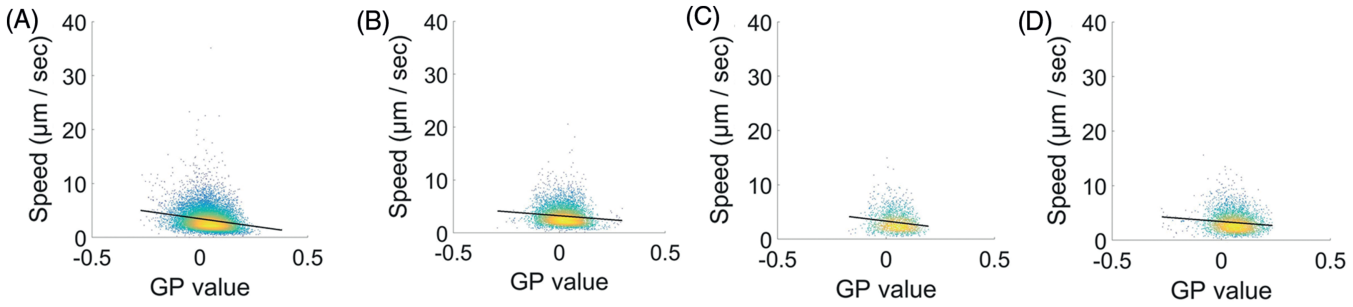

FIGURE 2 Vesicle order (GP) and track speed correlations for individual vesicles in primary human T cell synapses. Tracking statistics from individual vesicles aggregated from multiple cells for control conditions (A), Cytochalasin-D treatment (B), Jasplakinolide (C) and Nocodazole (D) correlating GP values with vesicle velocity. Data acquired from a minimum of n = 10 cells per condition

cells. However, Jasplakinolide-treated cells did not display a difference in the value of the correlation (gradient between −0.96 and −0.58; 95% CI). These results are also summarized in Figure S3.

The cytoskeletal modulating drugs led to shifts in the observed GP values of aggregated data (Figure S4), here Cytochalasin-D led to reduced GP values, while Jasplakinolide and Nocodazole treatments led to increased GP values possibly by changing the population of vesicles that can access the synapse interface.

Correlation analysis therefore demonstrated that disrupting actin or microtubule fibres led to a scrambling of the relationship between vesicle GP values and their velocities. In control conditions, high-order vesicles move slower than low-order vesicles, but the strength of this trend is reduced by both Cytochalasin-D and Nocodazole treatment; implying both cytoskeletal components are required to maintain the differential in velocities between high- and low-ordered vesicles. To further test whether high- and low-order vesicles differentially interacted with the actin and tubulin cytoskeletal components, we performed 3-channel confocal microscopy.

2.2 | Vesicles differentially associate with the actin and tubulin cytoskeletons

Vesicles within Jurkat T cells were labelled with the environmentally sensitive dye di-4-ANEPPDHQ and imaged using a confocal microscope (see *Methods* section). After synapse formation against an antibody-coated coverslip, the cells were fixed and the actin or microtubule networks were labelled. A representative ordered channel vesicle image (Figure 3A), disordered channel image (Figure 3B) and actin cytoskeleton image (Figure 3C) are shown. Actin imaging showed the well-characterized dense meshwork at peripheral regions giving way to resolvable fibres towards the synapse centre. The 3-channel merged image is shown in Figure 3D. Note that due to being acquired on different systems, the absolute GP values are not comparable between TIRF (Figures 1 and 2) and confocal image data. Correlation analysis (Figure 3E) revealed individual vesicle GP values were not correlated with local actin intensity (R^2 < 0.001, with a goodness of fit F-score of 0.374 [P > .05], n = 1635). Imaging was repeated with labelled vesicles and microtubules (Figure 3F-I). The microtubule organising centre (MTOC) localized near the synapse centre, where the actin-poor region is also located. Correlation analysis was carried out (Figure 3J), revealing individual vesicle GP values were positively correlated to local microtubule density (R^2 < 0.005, with a goodness of fit F-score of 8.686 [P < .005], n = 4129), implying microtubules might preferentially traffic high-order vesicles.

Together, these results demonstrate low-order vesicles exhibit faster dynamics and may be located between actin fibres, while vesicles located on microtubules are more ordered and demonstrate slower movement.

2.3 | Vesicle lipid order correlates with cargo

Lipid order has been shown to contribute to protein heterogeneity within the PM, including that at the T cell synapse.[24,25] Here, vesicles have been shown to exhibit order heterogeneity akin to the PM; it was therefore hypothesized that vesicles of different lipid order may contain different cargo proteins important for T cell signalling and for regulating vesicle transportation. Firstly, LAT, which is known to reside both in the PM and vesicles,[13,26,27] was imaged alongside vesicles to establish whether vesicular LAT correlated with a specific subsynaptic vesicle population based on lipid order. Images of vesicles and LAT within Jurkat T cells (Figure 4A-C) demonstrate populations of LAT did not fully overlay with vesicle staining (Figure 4D); agreeing with previous literature that 2 populations exist. Correlation analysis of individual vesicles revealed LAT weakly but significantly correlated with more ordered vesicle structures (Figure 4E; R^2 > 0.005, with a goodness of fit F-score of 71.29 [P < .0001], n = 3794). Finally, vesicle lipid order was imaged alongside MAL which is known to mediate vesicle trafficking to the synapse interface[11] (Figure 4F-I). Correlation analysis revealed MAL did not preferentially segregate into order-dependent vesicular structures at the IS, based on lipid order (Figure 4J; R^2 > 0.005, with a goodness of fit F-score of 3.615 [P > .05], n = 516).

3 | DISCUSSION

The machinery required to traffic vesicles to the IS is largely unknown. Recent work has investigated trafficking regulators such as the Rab GTPases and SNARE proteins within the context of vesicle cargo,[11] however, separate vesicle subpopulations as determined by their cargo do not share trafficking regulators.[28] How all these vesicles are trafficked to the synapse interface requires further investigation.

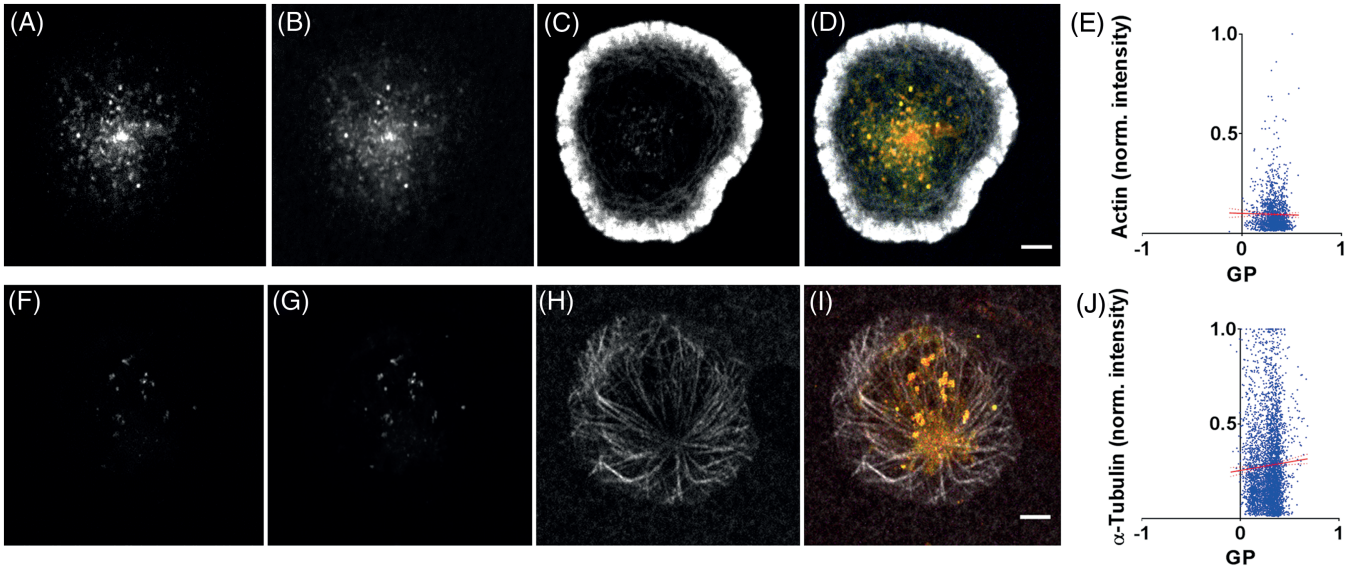

FIGURE 3 Vesicle lipid order and the cytoskeleton at the immunological synapse of Jurkat T cells. Vesicles were stained with di-4-ANEPPDHQ to permit imaging of both (A) ordered and (B) disordered channels. Actin (C) was visualized allowing overlay with vesicle data (D). Individual vesicle GP values from multiple cells were correlated against local actin intensity, providing a non-significant correlation (E). Vesicles were then stained with di-4-ANEPPDHQ to permit imaging of both (F) ordered and (G) disordered channels. Microtubules (H) were visualized allowing overlay with vesicle data (I). Individual vesicle GP values from multiple cells were correlated against microtubule intensity providing a significantly non-zero correlation (J). Scale bars = 5 μm

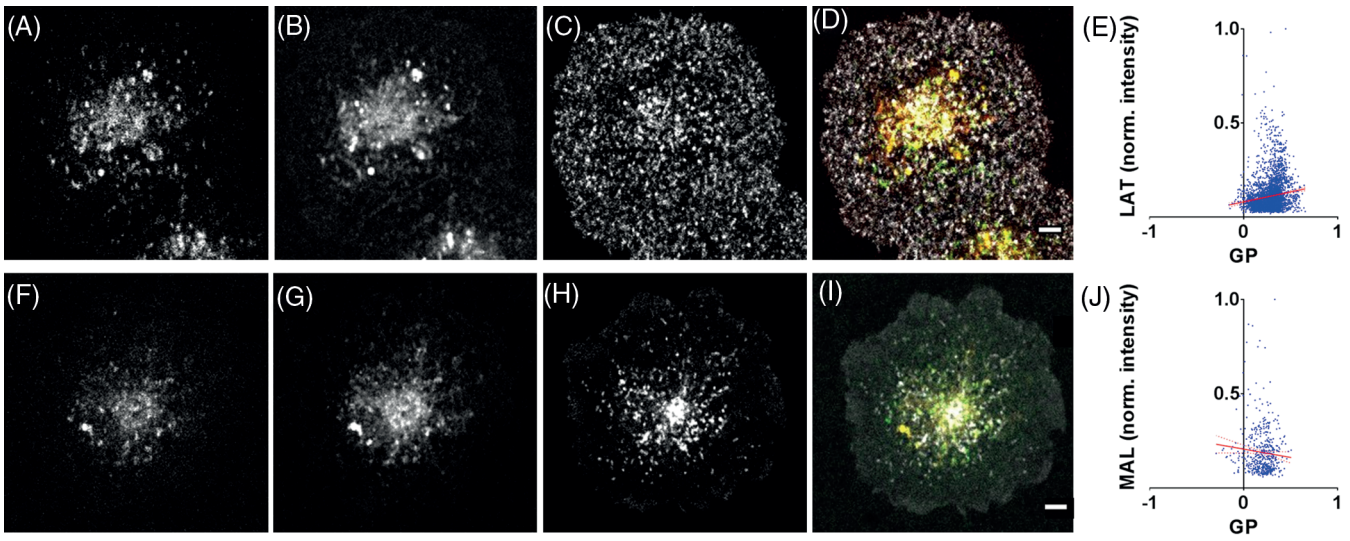

FIGURE 4 Vesicle lipid order and cargo at the Jurkat T cell immunological synapse. Vesicles were stained with di-4-ANEPPDHQ to permit imaging of both (A) ordered and (B) disordered channels. LAT (C) was visualized allowing overlay with vesicle data (D). Individual vesicle GP values from multiple cells were correlated against LAT intensity providing a significantly non-zero correlation (E). Vesicles were stained with di-4-ANEPPDHQ to permit imaging of both (F) ordered and (G) disordered channels. MAL (H) was visualized allowing overlay with vesicle data (I). Individual vesicle GP values from multiple cells were correlated against MAL intensity providing a non-significant correlation (J). Scale bars = 5 μm

It has been previously shown that MAL-containing vesicles can move along microtubules and transport the src-family kinase lymphocyte-specific protein tyrosine kinase (Lck) to the PM, while knockdown of the actin modulating protein Inverted Formin2 leads to impaired MAL-containing vesicle formation.[29] This work demonstrates the complex interplay between the cytoskeleton, vesicular trafficking and specific molecular cargo, which we have investigated further here.

This study has outlined the combination of live-cell imaging and analysis techniques for the novel quantification of synaptic vesicles, characterising their lipid order, dynamics, cargo and co-localisation with cytoskeletal components. In the context of primary human T cells, vesicles were shown to exhibit correlations between lipid order and track dynamics; with more disordered vesicles exhibiting faster speeds compared to ordered vesicles. More ordered vesicles were preferentially located on microtubules with the correlation between

lipid order and velocity diminished upon disruption of microtubules by Nocodazole. It was also shown that LAT preferentially segregates into more ordered vesicles, as expected[19] whereas MAL did not show any significant order-dependent enrichment. There is therefore a partial segregation of MAL and LAT which aligns with previous findings that MAL may not be present in LAT-containing vesicles.[11,21] A summary of these finding is shown in Figure 5.

Our results indicate that the role of membrane lipid order in regulating protein trafficking should be studied further. Not only is this a potential novel regulator of T cell signalling but may be a new application of the lipid raft hypothesis. Biochemical studies, such as detergent resistant membrane extraction and careful organelle extraction, coupled with proteomics and/or lipidomics would provide valuable new data in relation to our model (Figure 5). Overall, our findings demonstrate a complex interplay between sub-synaptic vesicles, membrane order, and their localisation to the cytoskeleton and how the cargo they contain may modulate synaptic delivery and localisation. This lipid order-based segregation of cargos may demonstrate a mechanism whereby scaffolding molecules and their signalosome partners are trafficked separately until incorporated into the PM for signal internalisation.

4 | MATERIALS AND METHODS

4.1 | Cell culture and synapse formation

Jurkat clone E6.1 T cells (ATCC) were cultured at 3×10^5 cells/mL in Roswell Park Memorial Institute media (Thermo Fisher) supplemented with 10% foetal bovine serum (FBS; Thermo Fisher) and 1% Penicillin Streptomycin (PenStrep; Thermo Fisher), at 37°C in a 5% CO_2 environment. Primary human T cells were isolated from human blood; cultured at 2×10^6 mL in Iscove's Modified Dulbecco's media (Thermo Fisher) supplemented with 10% FBS and 1% PenStrep. phytohaemagglutinin of 1 μg/mL or antibodies against human CD3 (Cambridge Bioscience) was then added to stimulate the T cells and drive clonal expansion.

ISs were formed against a stimulatory coverslip coated with CD3 and CD28 antibodies. 8-Well Ibidi (Ibidi) coverslips were coated the day before imaging, with 200 μL of PBS containing 1 μg/mL of human CD3 and 1 μg/mL of human CD28 antibody (BD Bioscience). Coated coverslips were stored at 4°C overnight. Prior to adding cells, coverslips were gently washed once with room temperature PBS to remove any antibodies still in suspension before 37°C Hanks' balanced salt solution (HBSS; Thermo Fisher) was added.

4.2 | Sample preparation

Jurkat and primary human T cells were stained with 5 μM di-4-ANEPPDHQ (Thermo Fisher) for 20 minutes. Cells were then resuspended in HBSS + 20 mM 4-(2-hydroxyethyl)-1-piperazineethanesulfonic acid (HEPES; Thermo Fisher) to reduce PM staining but leaving internal membranous components including vesicles stained. Cells were then pipetted onto coverslips for imaging at 3×10^4 to 4×10^4 cells/mL. For live cell experiments, coated coverslips were pre-heated in the microscope incubation chamber 30 minutes prior to imaging.

For fixed 3-channel experiments, after synapse formation as above, Jurkat T cells were fixed 10 minutes after stimulation, for 20 minutes with 4% paraformaldehyde (Electron Microscopy Sciences) in an actin cytoskeletal buffer (10 mM MES [2-(N-morpholino) ethanesulphonic acid] at a pH of 6.1, 5 mM magnesium chloride, 5 mM EGTA [ethylene glycol tetraacetic acid], 150 mM sodium chloride and 5 mM glucose, with a final pH of 7.0) before being washed in PBS. Cells were then permeabilized for 10 minutes with 0.01% lysolecithin (Sigma-Aldrich) in PBS. Next samples were blocked for 1 hour at 37°C with 2% bovine serum albumin (Sigma-Aldrich) and 0.2% fish skin gelatin (Sigma-Aldrich) in PBS before adding antibodies and labels.

For 3-channel imaging of vesicles and actin in Jurkat T cells, Alexa Fluor 647-tagged phalloidin (Thermo Fisher) was added at a 1:200 dilution for 1 hour at room temperature. After washing 3 times with PBS cells were imaged. Microtubules were labelled through incubation for 1 hour at room temperature with the α-tubulin mouse anti-human antibody DM1A (Thermo-Fisher), followed by labelling with the secondary antibody rabbit anti-mouse conjugated to Alexa Fluor 647 (Life Technologies). After washing 3 times with PBS cells were imaged. LAT was imaged by incubation of mouse anti-human primary (Cell Signalling Technology) for 1 hour at room temperature, followed by labelling with a rabbit anti-mouse secondary conjugated to Alexa Fluor 647 (Life Technologies) for 1 hour at room temperature. After washing 3 times with PBS cells were imaged. For MAL, ER and Golgi imaging, T cells were transiently transfected using the Amaxa (Lonza) Nucleofector protocol 24 hours prior to imaging, using MAL-mCherry (gift from Dr Helena Soares), tdTomato-ER-3 or tdTomato-Golgi-7 (gifts from Davidson lab).

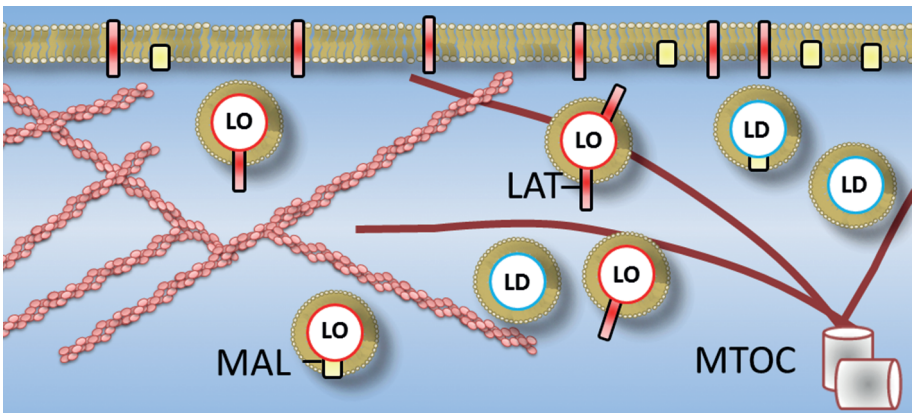

FIGURE 5 Schematic diagram of vesicle lipid order, cytoskeletal components and cargo at the T cell immunological synapse. More ordered (L_o) vesicles preferentially contain LAT, while MAL is more evenly distributed between vesicles. High-order (L_o) vesicles are preferentially associated with microtubules (in red) rather than the actin cytoskeleton (in pink)

4.3 | Imaging

Live-cell 2-channel vesicle imaging was carried out using a Nikon Ti-E wide field microscope, with a 1.49 NA ×60 Apo-TIRF oil immersion objective lens (Nikon) under TIRF illumination conditions using a 488 nm 50 mW laser (Coherent) set to 50% laser power. An OptiSplit III image splitter (Cairn) separated the ordered and disordered spectra for GP analysis. Separation of the ordered and disordered channels was provided by a 542/50 nm bandpass and 660 nm longpass filter setup (Semrock). Imaging was carried out at 4 frames per second, with signal captured using a sCMOS camera (Andor).

The 3-channel fixed cell imaging was carried out on a Nikon A1R confocal microscope using a CFI Apo ×100 1.49 objective lens (Nikon), imaging occurred sequentially using a 488 nm laser for membrane order (emission spectra was split using a 525/50 nm and 595/50 nm filter set). Far-red imaging with a 642 nm laser used a 700 nm longpass filter.

4.4 | Drug treatments

Five minutes after contact with a stimulatory coverslip, drugs were added directly to the primary human T cell-containing wells. Vesicles were imaged as with control experiments. Stock solutions of Cytochalasin-D (10 mM), Jasplakinolide (1 mM) and Nocodazole (10 mM) were dissolved in ethanol or dimethyl sulphoxide (DMSO) and stored at −20°C.

4.5 | Analysis

GP measurements were carried out as previously described.[30] Briefly, images for ordered and disordered channels were quantified by ratiometric analysis, giving a measure of membrane order. After GP analysis, generated grayscale images were combined with the merged ordered-disordered raw images; with merged image used to track vesicles. Vesicles were tracked semi-automatically using Imaris (v8.4.0, Bitplane), after identifying vesicle "spots" in each frame, using an estimated *x*, *y* diameter of 0.2 μm with a background subtraction and a filter "quality" of ≈2; based on visual inspection. For vesicle tracking the autoregressive motion algorithm was used, with tracks plotted for spots moving a maximum distance of 4 μm between frames. Vesicle track characteristics were then exported along with respective vesicle GP values for correlation analysis. Organelle and MAL tracking utilized the same settings as the vesicle data, however, the "quality" score was changed according to intercellular variability, based on visual inspection.

For correlation analysis of vesicle GP values and cytoskeletal components or protein cargo, regions of interest were selected on individual vesicles, followed by measurement of GP values and local cytoskeletal or cargo intensities. Vesicle-like structures were identified using the Squassh plugin for ImageJ.[31]

All image analysis was carried out in ImageJ. Statistical analysis was carried out in GraphPad Prism (v5.04, GraphPad Software Inc.). All data were reported as the mean ± standard deviation, with 2-tailed Student's *t* test analysis for condition comparison and confidence intervals set to 99%. Correlation analysis of vesicle GP values and track characteristics used the Pearson correlation function, assuming a Gaussian distribution.

ACKNOWLEDGMENTS

D.M.O. acknowledges European Research Council Grant No. 337187 and the Marie-Curie Career Integration Grant No. 334303. The authors declare no conflicts of interest. MAL-mCherry was a gift from Dr Helena Soares, tdTomato-ER-3 and tdTomato-Golgi-7 were gifts from the Davidson lab.

Author contributions

G.W.A., D.J.W. and D.M.O. designed the experiments and wrote the manuscript, G.L.B. aided in sample preparation, G.W.A., G.S., N.D. and D.J.W. carried out the imaging experiments and analysis.

Editorial Process File:

The Editorial Process File is available in the online version of this article.

REFERENCES

1. Varma R, Campi G, Yokosuka T, Saito T, Dustin ML. T cell receptor-proximal signals are sustained in peripheral microclusters and terminated in the central supramolecular activation cluster. *Immunity*. 2006;25:117–127.
2. Valitutti S, Müller S, Cella M, Padovan E, Lanzavecchia A. Serial triggering of many T-cell receptors by a few peptide-MHC complexes. *Nature*. 1995;375:148–151.
3. Onnis A, Finetti F, Baldari CT. Vesicular trafficking to the immune synapse: how to assemble receptor-tailored pathways from a basic building set. *Front Immunol*. 2016;7:50.
4. Masi G, Baldari CT. Signaling at the immune synapse: vesicular trafficking takes the stage. *Cell Mol Immunol*. 2013;10:459–462.
5. Ritter AT, Asano Y, Stinchcombe JC, et al. Actin depletion initiates events leading to granule secretion at the immunological synapse. *Immunity*. 2015;42:864–876.
6. Neco P, Giner D, del Mar Francés M, Viniegra S, Gutiérrez LM. Differential participation of actin- and tubulin-based vesicle transport systems during secretion in bovine chromaffin cells. *Eur J Neurosci*. 2003;18:733–742.
7. Schuh M. An actin-dependent mechanism for long-range vesicle transport. *Nat Cell Biol*. 2011;13:1431–1436.
8. Lang T, Wacker I, Wunderlich I, et al. Role of actin cortex in the Subplasmalemmal transport of secretory granules in PC-12 cells. *Biophys J*. 2000;78:2863–2877.
9. Wang J, Richards DA. Spatial regulation of exocytic site and vesicle mobilization by the actin cytoskeleton. *PLoS One*. 2011;6:e29162.
10. Yuan T, Lu J, Zhang J, Zhang Y, Chen L. Spatiotemporal detection and analysis of exocytosis reveal fusion 'hotspots' organized by the cytoskeleton in endocrine cells. *Biophys J*. 2015;108:251–260.
11. Soares H, Henriques R, Sachse M, et al. Regulated vesicle fusion generates signaling nanoterritories that control T cell activation at the immunological synapse. *J Exp Med*. 2013;210:2415–2433.
12. Larghi P, Williamson DJ, Carpier JM, et al. VAMP7 controls T cell activation by regulating the recruitment and phosphorylation of vesicular Lat at TCR-activation sites. *Nat Immunol*. 2013;14:723–731.
13. Williamson DJ, Owen DM, Rossy J, et al. Pre-existing clusters of the adaptor Lat do not participate in early T cell signaling events. *Nat Immunol*. 2011;12:655–662.
14. Choudhuri K, Llodrá J, Roth EW, et al. Polarized release of T-cell-receptor-enriched microvesicles at the immunological synapse. *Nature*. 2014;507:118–123.

15. Olsen BN, Bielska AA, Lee T, et al. The structural basis of cholesterol accessibility in membranes. *Biophys J*. 2013;105:1838–1847.
16. Klemm RW, Ejsing CS, Surma MA, et al. Segregation of sphingolipids and sterols during formation of secretory vesicles at the trans-Golgi network. *J Cell Biol*. 2009;185:601–612.
17. Mondal S, Johnston JM, Wang H, Khelashvili G, Filizola M, Weinstein H. Membrane driven spatial organization of GPCRs. *Sci Rep*. 2013;3(1–9):2909.
18. Milovanovic D, Honigmann A, Koike S, et al. Hydrophobic mismatch sorts SNARE proteins into distinct membrane domains. *Nat Commun*. 2015;6:5984.
19. Zhang W, Trible RP, Samelson LE. Palmitoylation: its essential role in membrane microdomain targeting and tyrosine phosphorylation during T cell activation. *Immunity*. 1998;9:239–246.
20. Frank M. MAL, a proteolipid in glycosphingolipid enriched domains: functional implications in myelin and beyond. *Prog Neurobiol*. 2000;60:531–544.
21. Anton OM, Andres-Delgado L, Reglero-Real N, Batista A, Alonso MA. MAL protein controls protein sorting at the supramolecular activation cluster of human T lymphocytes. *J Immunol*. 2011;186:6345–6356.
22. Jin L, Millard AC, Wuskell JP, Clark HA, Loew LM. Cholesterol-enriched lipid domains can be visualized by di-4-ANEPPDHQ with linear and nonlinear optics. *Biophys J*. 2005;89:L04–L06.
23. Obaid AL, Loew LM, Wuskell JP, Salzberg BM. Novel naphthylstyryl-pyridium potentiometric dyes offer advantages for neural network analysis. *J Neurosci Methods*. 2004;134:179–190.
24. Owen DM, Williamson DJ, Magenau A, Gaus K. Sub-resolution lipid domains exist in the plasma membrane and regulate protein diffusion and distribution. *Nat Commun*. 2012;3:1256.
25. Dinic J, Riehl A, Adler J, Parmryd I. The T cell receptor resides in ordered plasma membrane nanodomains that aggregate upon patching of the receptor. *Sci Rep*. 2015;5:10082.
26. Balagopalan L, Barr VA, Kortum RL, Park AK, Samelson LE. Cutting edge: cell surface linker for activation of T cells is recruited to microclusters and is active in signaling. *J Immunol*. 2013;190:3849–3853.
27. Bonello G, Blanchard N, Montoya MC et al. Dynamic recruitment of the adaptor protein LAT: LAT exists in two distinct intracellular pools and controls its own recruitment. *J Cell Sci*. 2004;117:1009–1016.
28. Fukuda M. Membrane traffic in the secretory pathway. *Cell Mol Life Sci*. 2008;65:2801–2813.
29. Andres-Delgado L, Anton OM, Madrid R, Byrne JA, Alonso MA. Formin INF2 regulates MAL-mediated transport of Lck to the plasma membrane of human T lymphocytes. *Blood*. 2010;116:5919–5929.
30. Owen DM, Rentero C, Magenau A, Abu-Siniyeh A, Gaus K. Quantitative imaging of membrane lipid order in cells and organisms. *Nat Protoc*. 2011;7:24–35.
31. Rizk A, Paul G, Incardona P, et al. Segmentation and quantification of subcellular structures in fluorescence microscopy images using Squassh. *Nat Protoc*. 2014;9:586–596.

SUPPORTING INFORMATION

Additional Supporting Information may be found online in the supporting information tab for this article.

How to cite this article: Ashdown GW, Williamson DJ, Soh GHM, Day N, Burn GL, Owen DM. Membrane lipid order of sub-synaptic T cell vesicles correlates with their dynamics and function. *Traffic*. 2018;19:29–35. https://doi.org/10.1111/tra.12532